

For Publisher's use

POLARIZED STRUCTURE FUNCTIONS AND SPIN PHYSICS

UTA STÖSSLEIN

*Nuclear Physics Laboratory, University of Colorado at Boulder,
Campus Box 390, Boulder, CO 80309-0390, USA
E-mail: uta.stoesslein@desy.de*

Recent progress in the field of spin physics of high energy particle interactions is reviewed with particular emphasis on the spin structure functions as measured in polarized deep inelastic lepton-nucleon scattering (DIS). New measurements are presented to obtain more direct information on the composition of the nucleon angular momentum, with results from semi-inclusive DIS accessing flavour-separated parton distribution functions (PDF) and with first data from hard exclusive reactions which may be interpreted in terms of recently developed generalizations of parton distribution functions (GPD). Finally, experimental prospects are outlined which will lead to a further development of the virtues of QCD phenomenology of the spin structure of the nucleon.

1 Introduction

The understanding of strong interactions including spin as an additional degree of freedom is an intensively discussed question since Quantum Chromodynamics (QCD) became the gauge field theory of the strong interaction establishing the intuitive quark model as the valid concept for the nucleon substructure.

The quark-parton-model (QPM) could successfully explain the positive cross section asymmetries observed in deep inelastic polarized electron-proton experiments performed early at SLAC ^{1,2}. The modern age in QCD spin physics began when at CERN a high energy muon beam experiment accessed spin phenomena in an extended kinematic range of the four-momentum transfer squared Q^2 and Bjorken- x . The well-known result was the discovery, made in 1987 by the EMC experiment ³, that only a small fraction, $\frac{1}{2}\Delta\Sigma = \frac{1}{2}(0.12 \pm 0.17)$, of the proton's spin is due to the spin of quarks, contrary to expectations of the naive QPM ($\Delta\Sigma = 1$) or the relativistic QPM ($\Delta\Sigma = 0.58$). Perturbative QCD (pQCD) in next-to-leading order (NLO) was able to attribute the small value of $\Delta\Sigma$ to the axial anomaly in the polarized

photon-gluon-scattering cross section, which depends on the factorization and renormalization scheme.

Meanwhile a wealth of experimental data using deep inelastic scattering of polarized lepton beams off polarized targets has been taken at SLAC ^{4,5,6,7,8}, CERN ⁹ and DESY ^{10,11} which confirms $\Delta\Sigma$ to be small with typical values of about 0.2-0.4. The old question thus remains unanswered yet: Where is the remainder of the nucleon spin? Is it measurable and calculable? How important are non-perturbative effects of QCD which are immediately related to low energy physics and confinement? Which role are contributions from gluons or sea quarks playing as well as the orbital angular momentum of quarks and gluons? Are there new observables which could help to answer some of these questions?

In this report the recent progress in QCD spin physics is summarized, highlighting new precise data for the spin structure functions g_1 and g_2 from SLAC, HERMES and JLAB, updated estimates of polarized quark and gluon polarizations from NLO pQCD evolution, and more directly from interpreting semi-inclusive HERMES data in LO pQCD. First data from JLAB and HERMES on hard

exclusive processes are presented here, which potentially represent a unique experimental input to be used in conjunction with further polarized DIS data to identify the quark orbital angular momentum contribution to the nucleon spin.

New single-spin azimuthal asymmetry measurements from Hermes are presented. These suggest the yet unknown leading twist transversity distribution functions are accessible using transversely polarized targets at Hermes and protons at RHIC in the near future. Spin physics in polarized pp-collisions at RHIC opens new ways to determine the gluon polarization and also flavour separated quark spin distributions, complementary to data expected to come from the COMPASS experiment at CERN and from Hermes at DESY.

2 Experiments and Kinematics

The high energy facilities and experiments investigating the nucleon spin structure using polarized charged lepton beams and polarized targets are summarized in Tab. 1, where typical beam and target parameters are listed. The values achieved reflect the enormous development in target and beam technology over the last three decades. Besides the high values for the beam and target polarizations, of about 0.5 to 0.9, the factor f enters additionally as a dilution of polarization dependent quantities; it denotes the fraction of polarizable target material. For typical solid state target materials, as used at SLAC and CERN, f is small and varies from about 0.13 for butanol to 0.5 for lithium deuteride and is about 0.55 for a ${}^3\text{He}$ gas target (E154). The Hermes experiment has an internal target with almost pure gases where f is close to unity. The polarization as well as the f values, in conjunction with beam intensity and target thickness determine the statistical precision, which is largest for the E154/E155 experiments at the high-intensity

48 GeV SLAC electron beam and lower for SMC. The high beam energy of the CERN muon beam provided access to low Bjorken- x ($x < 0.01$) and to larger values of Q^2 ($Q^2 > 10 \text{ GeV}^2$).

The kinematic coverage of the fixed target experiments is essentially determined by the incoming beam energy E defining the squared centre-of-mass energy $s = 2ME$ which limits the maximum $Q^2 = 4EE' \sin^2 \theta/2$ to $Q_{\max}^2 = s$. The scaling variables Bjorken- x and inelasticity y are given by $x = Q^2/2M\nu$ and $y = \nu/E$, where M is the nucleon mass and $\nu = E - E'$ is the energy transferred by the virtual photon to the target nucleon. The energy E' and the polar angle θ of the scattered charged beam lepton determine the DIS kinematics. To cover also the higher Q^2 values, the E155/E155X experiments were performed with three independent magnetic spectrometers at central angles of 2.75° , 5.5° , and 10.5° . The SMC and Hermes spectrometers have a large acceptance in the forward direction which allows for semi-inclusive measurements.

The experiments complement each other in their sensitivity to possible systematic uncertainties associated in particular with the beam and target polarization; these are typically controlled at the level of 2 to 5%. For instance, different attempts were made to minimize instrumental asymmetries: SMC used two target cells with opposite polarization simultaneously, while the polarization of the Hermes gas target, which can be inverted within milliseconds, was flipped in cycles. At SLAC the helicity for each beam pulse was randomly selected. Whereas SLAC experiments and SMC determined the polarization of the target material P_T by nuclear magnetic resonance measurements, Hermes is using a Breit-Rabi-Polarimeter (for p,d). Also the beam polarimetry is rather different. The beam polarization P_B was determined using Møller scattering from polarized atomic electrons at SMC and SLAC experiments, but

Lab	Experiment	Year	Beam	P_B	Target	P_T	f
SLAC	E80 ¹	75	10-16 GeV e^-	0.85	H-butanol	0.50	0.13
	E130 ²	80	16-23 GeV e^-	0.81	H-butanol	0.58	0.15
	E142 ⁴	92	19-26 GeV e^-	0.39	³ He	0.35	0.35
	E143 ⁵	93	10-29 GeV e^-	0.85	NH ₃	0.70	0.15
					ND ₃	0.25	0.24
	E154 ⁶	95	48 GeV e^-	0.83	³ He	0.38	0.55
	E155 ⁸	97	48 GeV e^-	0.81	NH ₃	0.80	0.15
	E155X ¹²	99	29/32 GeV e^-	0.83	LiD	0.22	0.36
CERN	EMC ³	85	200 GeV μ^+	0.79	NH ₃	0.78	0.16
	SMC ⁹	92	100 GeV μ^+	0.81	D-butanol	0.40	0.19
		93	190 GeV μ^+	0.80	H-butanol	0.86	0.12
		94/95		0.80	D-butanol	0.50	0.20
		96		0.80	NH ₃	0.89	0.16
DESY	HERMES ^{10,11,13}	95	28 GeV e^+	0.55	³ He	0.46	1.0
		96/97		0.55	H	0.88	1.0
		98	28 GeV e^-	0.55	D	0.85	1.0
		99/00	28 GeV e^+	0.55	D	0.85	1.0
DESY	HERMES ¹⁴	≥ 01	28 GeV e^\pm	0.55	H	0.85	1.0
CERN	COMPASS ^{15,16}	≥ 01	160 GeV μ^+	0.80	NH ₃	0.90	0.16
					LiD	0.50	0.50
BNL	RHIC ¹⁷	≥ 01	200 GeV p	0.70	200 GeV p	0.70	1.0

Table 1. High energy spin physics experiments.

at Hermes utilizing the spin dependence of Compton backscattering of circularly polarized photons off polarized electrons.

In 2001, with COMPASS at the CERN high-intensity muon beam line M2 and Hermes Run II at DESY, two powerful fixed target experiments are operational. The recent commissioning of the polarized proton rings at RHIC is an important milestone in experimental spin physics. Two large collider detectors, PHENIX ¹⁸ and STAR ¹⁹, along with several smaller experiments, will participate in the RHIC spin programme.

3 Asymmetries and Structure Functions g_1 and g_2

Measurements of polarized nucleon structure functions in inclusive DIS have been traditionally a prime focus of spin physics experiments. Using longitudinally polarized charged lepton beams and polarized targets the helicity-dependent quark distributions can be probed. This sensitivity re-

sults from angular momentum conservation, i.e. virtual photons can only be absorbed by a quark if their spins are oriented antiparallel. In the naive QPM helicity-averaged and helicity-dependent quark momentum distribution functions are introduced

$$q(x) = q^+(x) + q^-(x), \quad (1)$$

$$\Delta q(x) = q^+(x) - q^-(x), \quad (2)$$

which are directly related to the spin-averaged structure function F_1 and the spin-dependent structure function g_1

$$F_1(x) = \frac{1}{2} \sum_q e_q^2 q(x), \quad (3)$$

$$g_1(x) = \frac{1}{2} \sum_q e_q^2 \Delta q(x). \quad (4)$$

Here the sums extend over both quark and anti-quark flavors weighted by the electrical charge e_q squared. The notations $q^{(+/-)}$ refer to parallel (antiparallel) orientation of the quark and nucleon spins. The second leading twist spin structure function g_2 measurable

in DIS is expected to be zero in the naive QPM.

The experimentally asymmetries accessible with a longitudinally polarized charged lepton beam are defined as ^a

$$A_{||} = \frac{\sigma_{\vec{\rightarrow}} - \sigma_{\vec{\leftarrow}}}{\sigma_{\vec{\rightarrow}} + \sigma_{\vec{\leftarrow}}}, \quad A_{\perp} = \frac{\sigma_{\downarrow\rightarrow} - \sigma_{\uparrow\rightarrow}}{\sigma_{\downarrow\rightarrow} + \sigma_{\uparrow\rightarrow}}, \quad (5)$$

where $\sigma_{\vec{\rightarrow}}$ ($\sigma_{\vec{\leftarrow}}$) is the cross section for the lepton and nucleon spins aligned parallel (anti-parallel), while $\sigma_{\downarrow\rightarrow}$ ($\sigma_{\uparrow\rightarrow}$) is the cross section for nucleons transversely polarized w.r.t. the beam spin orientation. These cross section asymmetries are related to two virtual photon asymmetries, A_1 and A_2 , through

$$A_{||} = D(A_1 + \eta A_2), \quad A_{\perp} = d(A_2 - \zeta A_1) \quad (6)$$

The factors D and d denote the virtual photon polarization where $D \approx y$. They are explicitly given by $D = [1 - (1 - y)\epsilon]/(1 + \epsilon R)$, which depends on the ratio of longitudinal to transverse virtual-photon absorption cross sections $R = \sigma_L/\sigma_T$, and by $d = D\sqrt{2\epsilon/(1 + \epsilon)}$. The quantity $\epsilon = [4(1 - y) - \gamma^2 y^2]/[2y^2 + 4(1 - y) + \gamma^2 y^2]$ describes the flux ratio of longitudinal to transverse photons. The kinematic factors are defined as $\eta = \epsilon\gamma y/[1 - \epsilon(1 - y)]$, $\gamma = 2Mx/\sqrt{Q^2}$ with $\eta \approx \gamma \frac{Q^2 \gg M^2}{0}$, and $\zeta = \eta(1 + \epsilon/2\epsilon)$.

The virtual photon asymmetries are bound by $|A_2| \leq \sqrt{R(1 + A_1)/2}$ ²⁰ and $|A_1| \leq 1$. They can be described in terms of the spin-dependent structure functions

$$A_1 = \frac{g_1 - \gamma^2 g_2}{F_1} \approx \frac{g_1}{F_1}, \quad (7)$$

$$A_2 = \gamma \frac{g_1 + g_2}{F_1}, \quad (8)$$

where $F_1 = F_2(1 + \gamma^2)/2x(1 + R)$ can be determined from measurements of R and of the well-known unpolarized structure function F_2 . From Eq. 7 one can deduce that use of longitudinally polarized target predominantly determines g_1 , while DIS experiments

^aHere the factor $1/P_B P_T f$ which accounts for dilution and for beam and target polarizations, see Sec. 2, is set to unity for the sake of simplicity.

using a transversely polarized target are sensitive to $g_1 + g_2$.

The extraction of the proton structure function g_1^P from a longitudinally polarized hydrogen target is straightforward. Extraction of the neutron structure function g_1^N from longitudinally polarized ^2H or ^3He targets, however, requires additional nuclear corrections to be applied. The polarization of the ^3He nucleus is mainly due to the neutron. Corrections due to the nuclear wave function of the polarized ^3He nucleus have to be applied using g_1^P data to evaluate the proton contributions, i.e.,

$$g_1^N(x, Q^2) = \frac{1}{\rho_n}(g_1^{^3\text{He}} - 2\rho_p g_1^P), \quad (9)$$

where $\rho_n = (0.86 \pm 0.02)$ and $\rho_p = (-0.028 \pm 0.004)$ are taken from a number of calculations ^{21,22}. Additional corrections due to the neutron binding energy and Fermi motion were shown to be small ²³. For the polarized deuteron, the large contribution due to the polarized proton must be subtracted. In addition the D-state component in the deuteron wave function will slightly reduce the deuteron spin structure function due to the opposite alignment of the p-n spin system in this orbital state. This leads to

$$g_1^N(x, Q^2) = \frac{2g_1^d(x, Q^2)}{(1 - 1.5\omega_D)} - g_1^P(x, Q^2), \quad (10)$$

where $\omega_D = 0.05 \pm 0.01$ ²⁴ is the D-state probability of the deuteron. Furthermore, a possible contribution may occur from the still unknown tensor-polarized structure function b_1^d , a new leading twist function that occurs in case of scattering electrons off a spin-1 target ²⁵. In the QPM, b_1 measures the difference in the quark momentum distributions of a helicity 1 and 0 target, i.e. $b_1 = \frac{1}{2}(2q_{\uparrow}^0 - q_{\uparrow}^1 - q_{\downarrow}^1)$. Here q_{\uparrow}^m (q_{\downarrow}^m) is the probability to find a quark with momentum fraction x and spin up (down) in a hadron or nucleus with helicity m . In all analysis so far $b_1^d = 0$ is assumed, but first data to constrain b_1^d are expected from Hermes ²⁶.

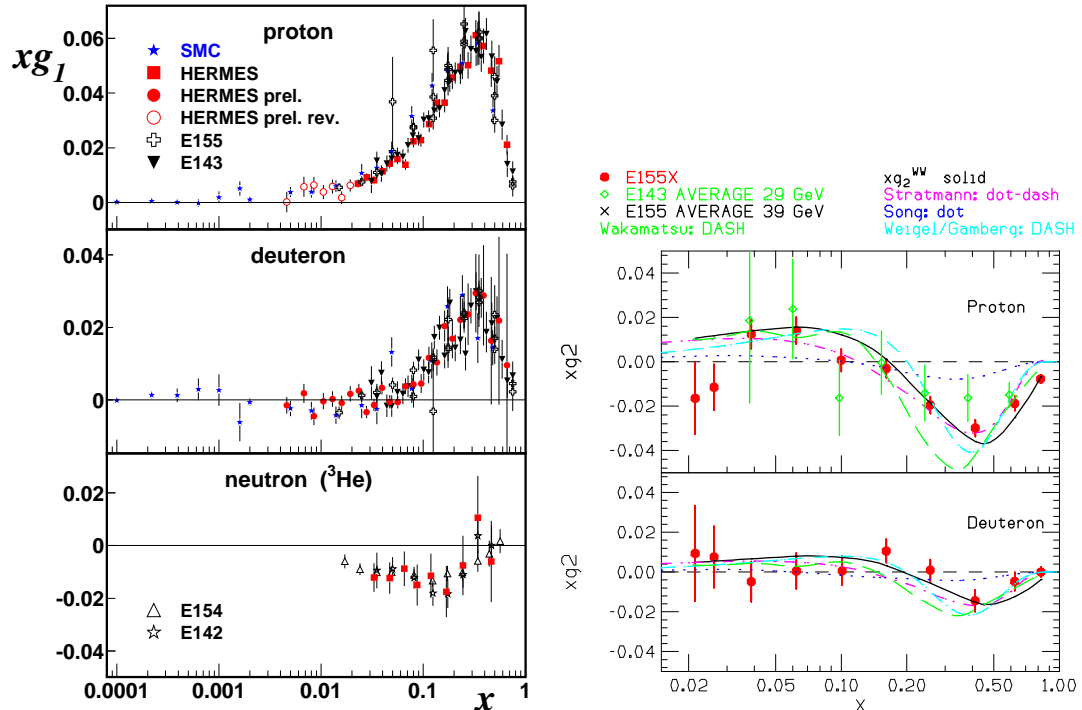


Figure 1. Compilation of recent data on the spin structure functions $xg_1(x, Q^2)$ (left) and $xg_2(x, Q^2)$ ¹² (right) including new data from HERA (Hermes preliminary) and SLAC (E155X). All data are given at their quoted mean Q^2 values. The values for xg_2 are compared with the g_2^{WW} term (solid line), see text, and several bag model calculations¹².

The recent world data on the spin structure functions $xg_1(x, Q^2)$ and $xg_2(x, Q^2)$ for the proton, deuteron and neutron are presented at their measured $\langle Q^2 \rangle$ values in Fig. 1. Also shown are the final high-precision data from E155, and new preliminary data from Hermes in the kinematic range $0.002 < x < 0.85$ and $0.1 \text{ GeV}^2 < Q^2 < 20 \text{ GeV}^2$, where the data at small Bjorken- $x < 0.01$ belong to low photon virtualities of $Q^2 < 1.2 \text{ GeV}^2$. These Hermes data confirm the SMC small- x and $Q^2 > 1 \text{ GeV}^2$ data for $A_1^{\text{p},\text{d}}$ for the first time. Even lower x values down to $x = 6 \cdot 10^{-5}$ but at extremely low $Q^2 = 0.01 \text{ GeV}^2$ were reached by SMC with a dedicated low- x trigger²⁷.

According to Fig. 1 the spin structure functions g_1 and g_2 are best known for the proton. The precision and kinematic coverage of the g_1 data is much better than for

the g_2 data. This holds even with the factor of three improved measurements of the dedicated E155X runs as compared to previous g_2 data from SMC²⁸ or from SLAC collaborations E142⁴, E143²⁹, E154³⁰ and E155³¹.

A comparison of xg_1 and xg_2 values leads to the striking observation that at high $x \sim 0.4$ the values of g_1 are positive and of g_2 are negative, but different from zero for both the proton and the deuteron. For g_2 , with so far limited accuracy, this is in contrast to the parton model expectation of $g_2 = 0$. There exists no simple partonic picture for $g_2 \neq 0$ which can be understood in terms of incoherent scattering of massless, collinear partons. It turns out that g_2 arises from higher-twist processes which can be described in terms of coherent parton scattering. The spin structure function g_2 is thus an interesting example for a higher-twist observable representing

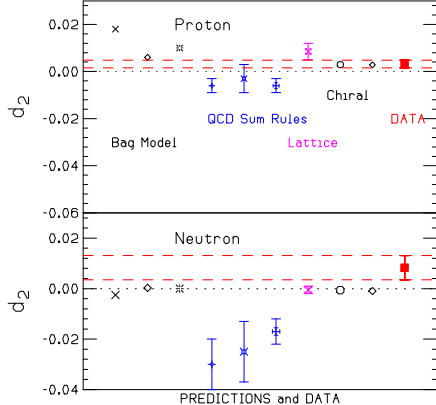


Figure 2. Calculations of the twist-3 matrix element d_2 of the proton and the neutron. The dashed lines indicate the present uncertainty in the data. Also shown are bag model, chiral quark model, QCD sum rule and recent QCD lattice calculations ¹².

quark-gluon correlations in the nucleon.

In fact, omitting quark mass terms, g_2 can be described by a twist-two contribution, the so-called g_2^{WW} Wandzura-Wilczek term ³² calculable from g_1 , and a pure twist-3 term denoted here with \bar{g}_2 reflecting the interaction-dependent part,

$$g_2(x, Q^2) = g_2^{\text{WW}} + \bar{g}_2(x, Q^2), \quad (11)$$

$$g_2^{\text{WW}}(x, Q^2) = -g_1(x, Q^2) + \int_x^1 \frac{g_1(y, Q^2)}{y} dy. \quad (12)$$

The recent data from the g_2 experiment E155X (right panel of Fig. 1) are in good agreement with the Wandzura-Wilczek approximation, $g_2^{\text{WW}} \propto -g_1$, which supports the observation discussed above. Consequently, any possible twist-3 term must be small. This is supported by new estimates ¹² of the twist-3 matrix element d_2 ,

$$d_2(Q^2) = 3 \int_0^1 x^2 [g_2(x, Q^2) - g_2^{\text{WW}}(x, Q^2)] dx, \quad (13)$$

obtained at an average Q^2 of 3 GeV² with an improved precision for the proton and the neutron, $d_2^p = 0.0032 \pm 0.0016$ and $d_2^n = 0.0083 \pm 0.0048$, respectively. Here, the g_2^{WW}

term was calculated using empirical fits ⁸ to g_1 data. The present status of d_2 measurements and model calculations is shown in Fig. 2. Further details about the complex nature of g_2 and d_2 may be found e.g. in Ref. ³³.

4 QCD Analyses and Gluon Polarization ΔG

QCD predicts the Q^2 dependence of unpolarized and polarized structure functions measured in DIS. Before discussing the theoretical framework and pQCD analyses of g_1 , it is worthwhile to look at the experimental status of measuring the Q^2 dependence of spin structure functions.

A compilation ⁸ of recent DIS data of the structure function ratio g_1/F_1 is shown in Fig. 3. In any given x bin, there is no experimental evidence of a strong Q^2 dependence of g_1/F_1 . A phenomenological fit to recent data with $Q^2 > 1$ GeV² and an energy of the hadronic final state $W > 2$ GeV, parametrizes a possible Q^2 dependence by ⁸

$$\frac{g_1^p}{F_1^p} = x^{0.700} (0.817 + 1.014x - 1.489x^2) \times (1 + \frac{c^p}{Q^2}) \quad (14)$$

$$\frac{g_1^n}{F_1^n} = x^{-0.335} (-0.013 - 0.330x + 0.761x^2) \times (1 + \frac{c^n}{Q^2}). \quad (15)$$

The coefficients $c^p = -0.04 \pm 0.06$ and $c^n = 0.13 \pm 0.45$ describing the Q^2 dependence found to be small and consistent with zero.

The transition from DIS to the low Q^2 regime, $Q^2 \lesssim 1$ GeV², and to the resonance region $W \lesssim 2$ GeV is investigated at TJ-NAF with beam energies of 0.8-5.7 GeV. Using polarized electrons ($P_B \sim 70\%$) scattered off polarized solid state targets significant, complementary measurements of g_1 and g_2 for $0.02 < Q^2 < 1.2$ GeV² are anticipated: first preliminary results for the asymmetry

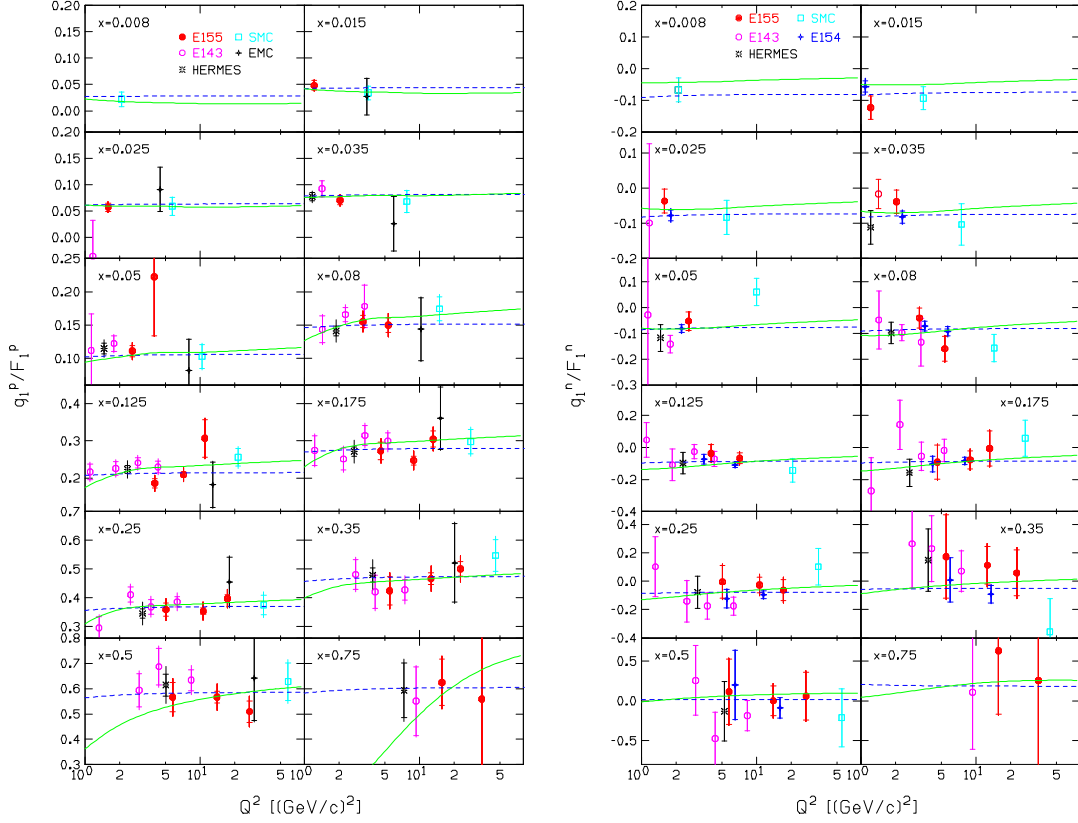


Figure 3. The Q^2 dependence of g_1/F_1 , note $g_1/F_1 \approx A_1$, of the proton (left) and neutron (right) for $Q^2 > 1 \text{ GeV}^2$ data. Also shown are the phenomenological fits (dashed line) and results from the E155 pQCD fit in NLO (dotted line)⁸.

$A_1 + \eta A_2$ are of remarkable statistical precision. The asymmetries show strong Q^2 dependences for a ${}^3\text{He}$ target³⁴ as well as for proton (NH_3) and deuteron (ND_3) targets³⁵. This behavior reflects the rapidly changing helicity structure of some resonances with the scale probed. Accurate measurements will allow stringent tests of nucleon structure models and may shed new light to the important question at which distance scale pQCD corrections will break down and physics of confinement may dominate.

While those tasks are still theoretically challenging, pQCD delivers a good description of the g_1 data with $Q^2 > 1 \text{ GeV}^2$. This is illustrated for the proton case in Fig. 4. The observed pattern of scaling violations of

g_1^p resembles the known pattern of scaling violation in the unpolarized structure function F_2^p . The Q^2 evolution equations, given in the DGLAP formalism, allow the unpolarized gluon distribution and the strong coupling constant α_s to be determined³⁶. Since gluons are vector particles they are expected to contribute to the spin of the nucleon as well, asymptotically about 50% of the protons spin.

In NLO pQCD, the spin structure function g_1 is given by

$$g_1^{p(n)} = \frac{1}{9} \left\{ \Delta C_{NS} \otimes \left[+(-)\frac{3}{4} \Delta q_3 + \frac{1}{4} \Delta q_8 \right] + \Delta C_S \otimes \Delta \Sigma + 2N_f \Delta C_G \otimes \Delta G \right\}, \quad (16)$$

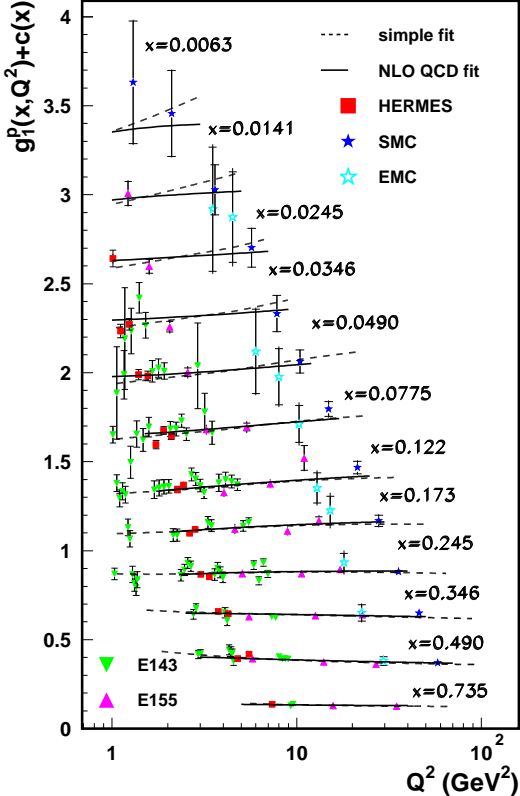


Figure 4. Q^2 dependence of $g_1^P(x, Q^2)$ for $Q^2 > 1$ GeV 2 . The g_1^P values are calculated using recent data on ratio g_1^P/F_1^P and the function F_1^P determined by F_2^P ³⁷ and R ³⁸. To evaluate the Q^2 behavior, the data has been shifted to common x values using F_1^P and g_1^P/F_1^P parameterizations. Also shown are the fit according to Eq. 14 and a NLO pQCD fit⁴¹.

where $\Delta C_{q,G}$ are the spin-dependent Wilson coefficients and \otimes denotes the convolution in x space. The usual notations for three flavours ($N_f = 3$) are:

$$\begin{aligned}\Delta\Sigma &= (\Delta u + \Delta \bar{u}) + (\Delta d + \Delta \bar{d}) + (\Delta s + \Delta \bar{s}) \\ \Delta q_3 &= (\Delta u + \Delta \bar{u}) - (\Delta d + \Delta \bar{d}) = 6(g_1^P - g_1^N) \\ \Delta q_8 &= (\Delta u + \Delta \bar{u}) + (\Delta d + \Delta \bar{d}) - 2(\Delta s + \Delta \bar{s}) \\ \Delta G & \quad \text{in NLO only; } \Delta C_G^0 = 0 \text{ in LO.}\end{aligned}$$

Apparently, inclusive data allow linear combinations of polarized PDFs ($\Delta q + \Delta \bar{q}$) and the gluon polarization ΔG , as an $\mathcal{O}(\alpha_s)$ correction, to be accessed by solving the DGLAP evolution equations. The mixing of the evolution of the quark singlet contribution $\Delta\Sigma$

and ΔG yields to renormalization and factorization scheme dependent results in NLO pQCD. Frequently used schemes are the $\overline{\text{MS}}$, Adler-Bardeen (AB) or JET schemes, see e.g. Ref.³⁹. In the AB and JET schemes, $\Delta\Sigma$ is conserved and defined to be a scale-independent quantity, which is related to the $\overline{\text{MS}}$ result by

$$\begin{aligned}\Delta\Sigma(Q^2)_{\overline{\text{MS}}} &= \Delta\Sigma_{\text{AB(JET)}} \\ &- N_f \frac{\alpha_s(Q^2)}{2\pi} \Delta G(Q^2).\end{aligned}\quad (17)$$

The polarized gluon distribution is the same in all these schemes, $\Delta G(Q^2)_{\overline{\text{MS}}} = \Delta G(Q^2)_{\text{AB(JET)}}$. Observed differences of ΔG values obtained might still point to systematic differences in the applied theoretical descriptions, which includes e.g. the treatment of quark masses and flavours, the use of the strong coupling constant α_s and the use of non-DIS data for further constraints, respectively.

Several groups have been performing spin-dependent NLO pQCD fits. The one performed by the SMC collaboration was the first to carefully treat statistical, systematic and theoretical uncertainties⁴⁰. A new attempt to propagate the statistical errors through the evolution procedure was done in Ref.⁴¹ and is presented in Fig. 5 together with other recent NLO fit results^{42,43}. The precise inclusive proton data predominantly constrain very well the up-valence quark polarization to be positive and confirm together with neutron and deuteron data the down-valence quark polarization to be negative. The polarized sea is determined to be negative while ΔG is suggested to be positive. However, both values have large uncertainties as illustrated with the bands in Fig. 5.

Spin-dependent pQCD analyses begin to become sensitive to the value of α_s as well. A recent determination of α_s yields $\alpha_s(M_z^2) = 0.114 \pm 0.005(\text{stat})^{+0.009}_{-0.006}(\text{scales})$ ⁴¹ which is consistent with the value obtained by SMC, $\alpha_s(M_z^2) = 0.121 \pm$

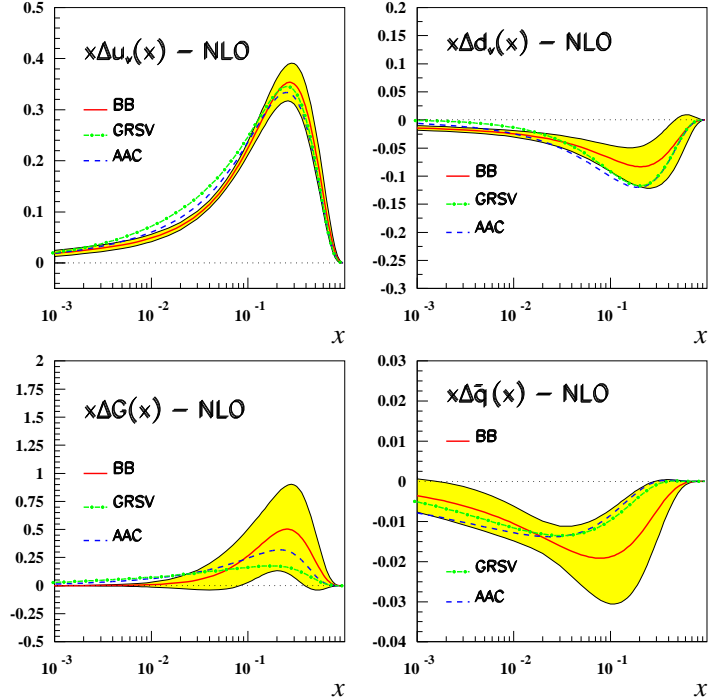


Figure 5. Polarized parton distribution functions $x\Delta d_V$, $x\Delta u_V$, $x\Delta G$ and $x\Delta \bar{q}$ from updated NLO pQCD (\overline{MS}) fits at $Q^2 = 4 \text{ GeV}^2$ using $SU(3)_f$ assumptions. Labels are according to the results from Ref. ⁴¹ (BB), Ref. ⁴² (GRSV), and Ref. ⁴³ (AAC). The shaded bands ⁴¹ represent the propagated statistical errors only.

$0.002(\text{stat}) \pm 0.006(\text{syst and thy})$ ⁴⁰.

Present pQCD analyses use information from neutron and hyperon β -decays to constrain the first moments of the non-singlet distributions (Δq_3 , Δq_8),

$$a_3 = \Delta q_3 = F + D = 1.267 \pm 0.0035 \quad (18)$$

$$a_8 = \Delta q_8 = 3F - D = 0.585 \pm 0.025. \quad (19)$$

Assuming $SU(3)_f$ flavour symmetry the first moment of g_1 is given by

$$\begin{aligned} \Gamma_1(Q^2) &= C_S(Q^2)a_0(Q^2) + \\ &+ C_{NS}(Q^2)\frac{1}{12}\left(\left|\frac{g_a}{g_v}\right| - \frac{1}{3}(3F - D)\right), \end{aligned} \quad (20)$$

where $|g_a/g_v|$ is the axial coupling constant and $a_0(Q^2)$ is the axial charge. An update of the E154 ⁴⁴ NLO pQCD fit in the \overline{MS} scheme was performed by the E155 collaboration ⁸ using published data. It further confirms the quark singlet contribution $\Delta\Sigma$ to be small, $\Delta\Sigma = 0.23 \pm 0.04(\text{stat}) \pm 0.06(\text{syst})$ at $Q^2 =$

5 GeV^2 , well below the Ellis-Jaffe prediction ⁴⁵ of 0.58. The value for $\Gamma_1^P - \Gamma_1^n = 0.176 \pm 0.003 \pm 0.007$ is found to be in agreement with the Bjorken sum rule prediction of 0.182 ± 0.005 . For the first moment of the gluon distribution a value of $\Delta G = 1.6 \pm 0.8(\text{stat}) \pm 1.1(\text{syst})$ is obtained, reflecting the fact, that the uncertainty on ΔG from scaling violations is still too large to significantly constrain the gluon contribution to the nucleon spin. The value of a_8 depends on the assumption of $SU(3)_f$ flavour symmetry among hyperons, which is known to be inexact. Indications of a breakdown of $SU(3)$ flavor symmetry, as observed in the hyperon β decay, and its impact on the polarized PDFs were discussed recently using the JET scheme ⁴⁶. While the influence on the singlet and non-strange quark polarizations was found to be small, the strange sea quark and gluon polarizations change significantly when $SU(3)_f$

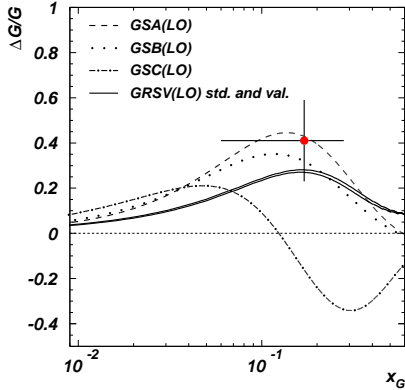


Figure 6. Hermes result⁴⁷ for $\Delta G/G$ extracted from high p_T unlike sign hadron pair production. The result is compared to LO pQCD fits to a subset of the world's data on g_1 : curves are from Refs.^{48,49} evaluated at $Q^2 = 2 \text{ GeV}^2$. The error bar on $\Delta G/G$ represents statistical and experimental systematic uncertainties only; no theoretical uncertainty is included.

symmetry breaking effects are considered⁴⁶: e.g. $\Delta s + \Delta \bar{s}$ varies from -0.02 to -0.15 and ΔG from 0.13 to 0.84 . The observed strong dependence of gluon and strange quark polarizations on the $SU(3)_f$ symmetry assumptions calls for more direct probes for a determination of those quantities.

A first attempt to determine $\Delta G/G$ from the photon-gluon fusion process (PGF) was presented by Hermes⁴⁷. Using a polarized hydrogen target and selecting events with two hadrons with opposite charge and high transverse momentum p_T , the double-spin asymmetry and its dependence on $p_T^{h_1}$ and $p_T^{h_2}$ was measured. For $h_1 h_2$ pairs with $p_T^{h_1} > 1.5 \text{ GeV}$ and $p_T^{h_2} > 1.0 \text{ GeV}$ the asymmetry is $A_{||} = -0.28 \pm 0.12 \text{ (stat)} \pm 0.02 \text{ (syst)}$. The result has been interpreted considering contributions from deep inelastic scattering, vector meson dominance and the two direct leading order QCD processes: PGF and QCD Compton scattering. Using the PYTHIA⁵⁰ program the relative cross section contributions were determined and the negative asymmetry explained by a positive gluon polarization. The asymmetry of the QCD Compton pro-

cess was calculated to be positive whereas the asymmetries of all other subprocesses were assumed to be zero. The extracted value of $\langle \Delta G/G \rangle = 0.41 \pm 0.18 \text{ (stat)} \pm 0.03 \text{ (syst)}$ is compared in Fig. 6 to several phenomenological LO pQCD fits where the hard scale of this process is given rather by $\langle p_T^2 \rangle = 2.1 \text{ GeV}^2$ and not by $\langle Q^2 \rangle$ of 0.06 GeV^2 . The positive sign of $\langle \Delta G/G \rangle$ at $\langle x_G \rangle = 0.17$ can only be altered by a large negative spin asymmetry from some neglected process, other than PGF.

A similar $\Delta G/G$ analysis is being performed by Hermes based on the high statistics deuteron data of the run periods 1998–2000⁵¹. The interpretation of such data is still limited to LO pQCD, since NLO simulation programs are not yet available.

5 Quark Polarizations from Semi-Inclusive Measurements

Information on the flavor separated polarized valence and sea quark contributions can possibly be obtained via semi-inclusive scattering, where one or more hadrons h in coincidence with the scattered charged lepton are detected. According to the favored fragmentation process, the charge of the hadron and its valence quark composition provide sensitivity to the flavor of the struck quark as is transparent within the QPM. Hence the double-spin asymmetries for hadrons, A_1^h , can be factored into separate z and x dependent terms,

$$A_1^h(x, Q^2) \approx \frac{g_1^h}{F_1^h}(x, Q^2) = \frac{\int_{z_{min}}^1 dz \sum_q e_q^2 \Delta q(x, Q^2) \cdot D_q^h(z, Q^2)}{\int_{z_{min}}^1 dz \sum_q e_q^2 q(x, Q^2) \cdot D_q^h(z, Q^2)}, \quad (21)$$

where the fragmentation function $D_q^h(z, Q^2)$ is the probability that the hadron h originated from the struck quark flavor q . Here $z = E_h/\nu$ is the hadron momentum fraction in the lab frame.

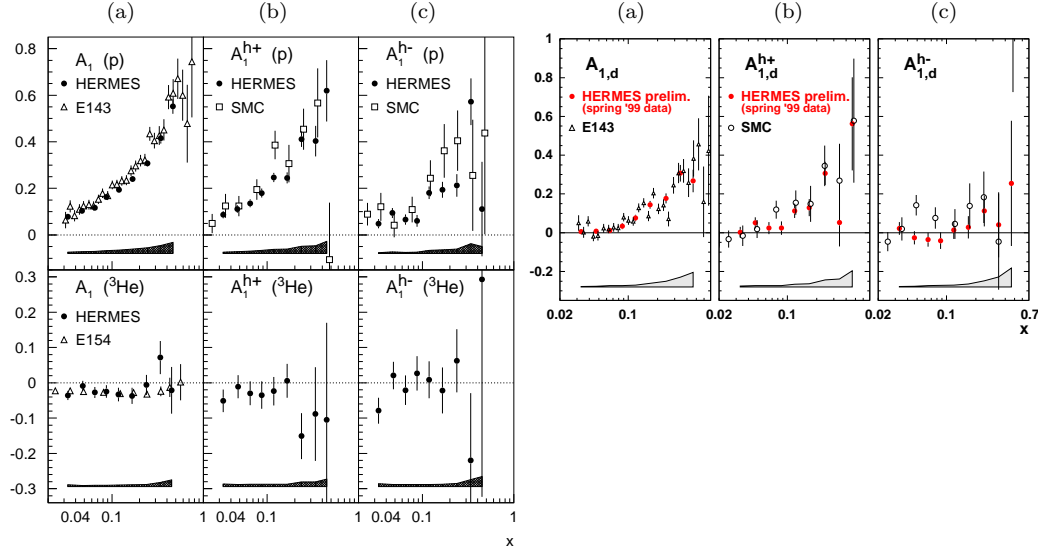


Figure 7. Inclusive (a) and semi-inclusive asymmetries for positively (b) and negatively (c) charged hadrons on the proton and ${}^3\text{He}$ targets (left) ⁵³ and on the deuterium target (right) ⁵⁴. The bands represent the systematic uncertainties of the HERMES data.

Results for semi-inclusive double-spin asymmetries measured with the large forward spectrometers of the SMC ⁵² and the HERMES ^{53,54} collaborations are shown in Fig. 7 including new preliminary data on the deuterium target. The inclusive data from HERMES in Fig. 7a are compared to SLAC (E143, E154) data. The results agree well which reflects the understanding of the experimental uncertainties. All data points at a given x have some mean Q^2 which differs for the HERMES, SLAC and the SMC experiments. The comparison of the semi-inclusive data, Figs. 7b and c, thus points to a rather weak Q^2 dependence. To maximize the sensitivity to the struck current quark, typically kinematic cuts of $W^2 > 10 \text{ GeV}^2$ and $z > 0.2$ are imposed on the data in order to suppress effects from target fragmentation.

According to Eq. 21, the double-spin asymmetries are sensitive to the quark polarizations weighted with unpolarized fragmentation functions. Following the HERMES analysis ⁵³, a *flavor tagging* probability may be determined by simulation using the LUND

string fragmentation model ⁵⁵. This allows in LO pQCD the polarized quark distributions to be extracted, see Fig. 8, using the measured asymmetries from the various targets. The present asymmetry set is most sensitive to the light valence quark polarizations (Δu_v , Δd_v) because of $u(d)$ -quark dominance: the production of h^\pm is dominated by scattering off $u(d)$ quarks from a proton(neutron) target. In particular, the impact of new HERMES deuterium data on the precision of Δd_v is clearly seen in Fig. 8. However, the sensitivity to the sea polarizations ($\Delta \bar{u}$, $\Delta \bar{d}$) is low, less than 10% at $x < 0.2$. Hence the sea polarization is assumed to be flavor independent in present analyses.

Fig. 8, as well as Fig. 5, represent the first moments at a fixed Q^2 which determine the flavor separated quark contributions to the nucleon spin: a positive (parallel to the nucleon spin) up quark and a negative (anti-parallel to the nucleon spin) down quark polarization are found. The polarization of the flavor undifferentiated sea is found to be com-

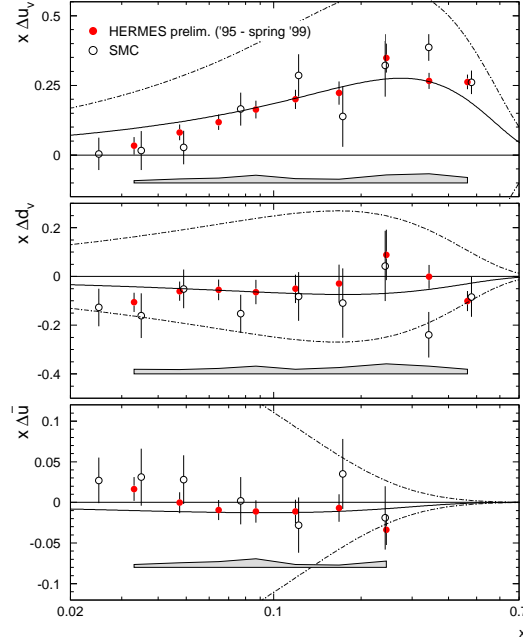


Figure 8. Parton spin distributions at $Q^2 = 2.5$ GeV^2 for the valence quarks $x\Delta u_v(x)$, $x\Delta d_v(x)$ and the sea quarks $x\Delta \bar{u}(x)$ as a function of x from SMC⁵² (data evolved to 2.5 GeV^2) and from Hermes with systematic uncertainty bands (preliminary)⁵⁴. The measurements are within the positivity limits given by the unpolarized quark distributions (dashed-dotted line) and are compared to parameterizations of the polarized quark distributions (solid line)⁴⁸.

patible with zero (see Fig.8). It is favored to be negative in spin-dependent NLO pQCD analyses (see Fig.5).

Theoretical conjecture (e.g. from the chiral Quark-Soliton-Model⁵⁶) and recent attempts towards a global analysis including semi-inclusive data (e.g. from Ref.⁵⁷) indicate a possible flavor asymmetry in the nucleon's light sea, $\Delta \bar{u} - \Delta \bar{d} \neq 0$, as in the unpolarized case. Current and future dedicated spin experiments are expected to vastly broaden the information necessary for a complete flavor separation. Further improvement in the knowledge of the sea polarizations will be soon available from the full high statistics set of Hermes deuterium data employing the pion and kaon identification capability of a RICH detector installed in 1998.

6 Exclusive Spin Physics

Based on impressive theoretical efforts in the last decade, for the first time a new window on the quark-gluon spin-structure of the nucleon was opened with a description of hard exclusive processes as deeply virtual Compton Scattering (DVCS) and meson production in QCD. For a recent review see e.g. Ref.⁵⁸. The framework of DIS is here extended to the non-forward region of the virtual Compton process. In the Bjorken limit the process may be viewed as factorizing in two steps: a hard interaction of the virtual photon with the nucleon, calculable in pQCD, and a soft interaction of the struck quark with other partons containing new non-perturbative information about the nucleon. The non-perturbative functions are the so-called generalized parton distribution functions. GPDs (usually denoted with

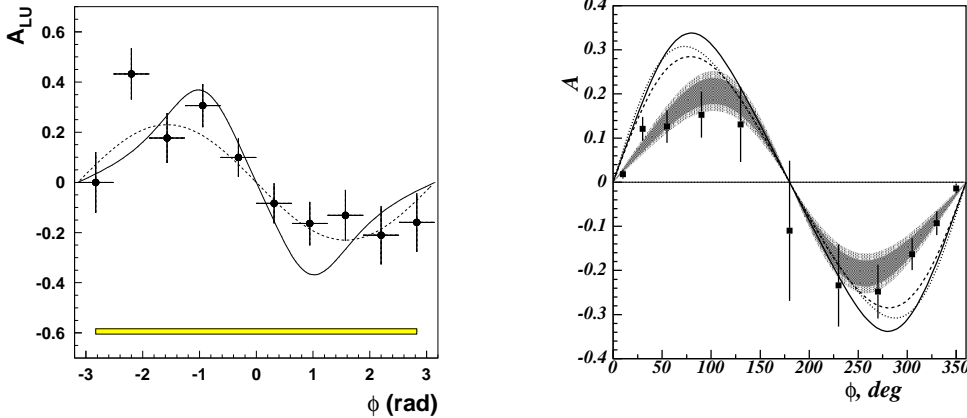


Figure 9. Single-spin asymmetry associated with DVCS as a function of ϕ from the HERMES ⁶⁴ (left) and from the CLAS ⁶⁵ (right) experiments. The curves represent model calculations. The shaded area (right) represents the uncertainties of the best phenomenological ϕ dependent fit functions. The subscripts L and U indicate the use of an longitudinally polarized beam and an unpolarized target, respectively.

$H, E, \tilde{H}, \tilde{E}$) represent probability amplitudes to knock out a parton from a nucleon and to put it back with a different longitudinal fraction of the momentum transfer ξ (skewness parameter). GPDs depend also on Q^2 and the squared momentum transfer to the nucleon t . These complex functions of multiple variables unify known concepts of hadronic physics, e.g. by linking ordinary parton distribution functions and nucleon form factors. In the context of spin physics, the attractive fact is that the total angular momentum J_q and J_G carried by a quark flavor and by a gluon, respectively, are given by the second moment of the sum of their unpolarized GPDs (H^q, E^q) in the limit $t = 0$ ⁵⁹. The total angular momenta of partons are still unknown and related by angular momentum conservation to the spin of the nucleon projected along an axis. The latter could be written also as a sum of contributions from quark ($\Delta\Sigma$) and gluon (ΔG) spin and orbital angular momentum of quarks (L_q) and of gluons

(L_g) ^{59,60}

$$\frac{1}{2} = J_q + J_g = \frac{1}{2} \Delta\Sigma + L_q + \Delta G + L_g. \quad (22)$$

To understand the composition of the nucleon spin finally, each contribution has to be identified. The usefulness of such angular momentum sum rule in the sense of a gauge invariant definition and measurability of each of the terms are yet under discussion ⁶¹, especially with respect to the gluon.

The DVCS channel is viewed to be a particular clean hadronic reaction that gives access to the GPDs ⁶². In the case of hard lepto-production of mesons, however, the theoretical description involves with the meson distribution amplitudes another unknown non-perturbative input, which may complicate the identification of the GPDs. So far, the experimental data and GPD models focus on the proton but GPDs for the deuteron were also introduced recently, see e.g. Ref ⁶³.

First experimental results on lepton beam helicity dependent asymmetries associated with DVCS were obtained from HERMES and confirmed by the CLAS col-

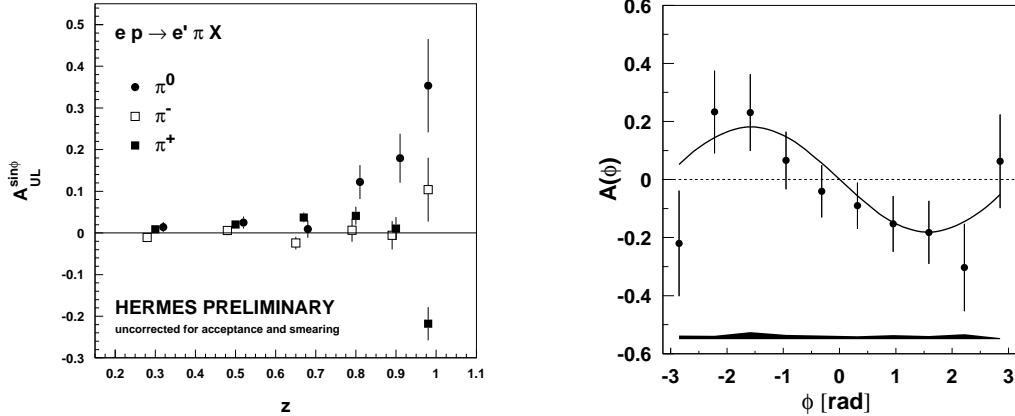


Figure 10. Hermes results on azimuthal $\sin\phi$ moments of the single-spin asymmetries measured for the production of charged and neutral pions, as a function of the pion momentum fraction z ⁶⁷ (left) and for the exclusive π^+ production⁶⁸ (right). Exclusive π^+ was selected by requiring the missing mass M_X of the reaction $e^+p \rightarrow e^+\pi^+X$ corresponded to the nucleon mass, $M_X < 1.05$ GeV. The curve is a fit to the data by $A(\phi) = A_{UL}^{\sin\phi} \cdot \sin\phi$. The subscripts U and L indicate the use of an unpolarized beam and a longitudinally polarized target, respectively.

laboration, see Fig. 9. This single-spin asymmetry is sensitive to the interference term formed from the imaginary part of the DVCS amplitude and the background QED Compton (Bethe-Heitler) amplitude, $d\sigma_{\leftarrow} - d\sigma_{\rightarrow} \propto \text{Im}(T_{\text{DVCS}})T_{\text{BH}}$. In a LO leading twist description, this leads to a $\sin\phi$ dependence in the related asymmetry, $A(\phi) = \alpha \text{sign}(e) \sin\phi$. Here, $\text{sign}(e)$ represents the sign of the beam charge and ϕ is the angle between the γ and e scattering planes. The integrated beam-spin asymmetry obtained from positron scattering off a hydrogen target at Hermes is $\alpha = -0.23 \pm 0.04(\text{stat}) \pm 0.03(\text{syst})$, while electron scattering at CLAS yields $\alpha = 0.202 \pm 0.021(\text{stat}) \pm 0.009(\text{syst})$. Both results are in fair agreement with a simple $\sin\phi$ dependence and a change in the sign is seen with the beam charge used. The restricted kinematic range do not allow to study dependencies on the relevant kinematic variables so far. It is for Hermes, $\langle Q^2 \rangle = 2.6$ GeV², $\langle \text{Bjorken-}x \rangle = 0.11$, and $\langle -t \rangle = 0.27$ GeV², while for CLAS it is $1 \text{ GeV}^2 < Q^2 < 1.75 \text{ GeV}^2$, $0.13 < \text{Bjorken-}x < 0.35$, and $0.1 \text{ GeV}^2 < -t < 0.3 \text{ GeV}^2$. Both ex-

periments will continue such measurements and more precise data are expected to become available. It will then particularly be interesting to test the significance of higher $\sin\phi$ moments which are sensitive to quark-gluon correlations as described by twist-three GPDs.

Since only a quadratic combination of GPDs appears in the unpolarized cross section, polarization is needed in order to disentangle the various distributions by accessing additional observables. For example, it has been predicted⁶⁶ that for the exclusive production of π^+ mesons from a transversely polarized target by longitudinally virtual photons, the interference between the pseudoscalar (\tilde{E}) and pseudovector (\tilde{H} with $\tilde{H} \rightarrow \Delta q$ in forward limit at $t = 0$) amplitudes leads to a large asymmetry in the distribution of the angle ϕ . Here ϕ is the azimuthal angle of the pion around the lepton scattering plane.

For the first time, the Hermes collaboration presented data on single-spin azimuthal asymmetries measured in the reaction $ep \rightarrow e'\pi X$ using longitudinally polarized protons^{67,68}, see Fig. 10. Compar-

ing the left and right panels of Fig. 10 it is clearly seen, that for π^+ production at high z (> 0.9) the $\sin\phi$ moment of the asymmetry is observed⁶⁷ to become suddenly negative, in agreement with a different (but related) analysis of exclusive π^+ data⁶⁸. A fit to the exclusive data, $A(\phi) = A_{\text{UL}}^{\sin\phi} \cdot \sin\phi$, delivers the $\sin\phi$ moment of the target-spin related asymmetry to be $A_{\text{UL}}^{\sin\phi} = -0.18 \pm 0.05(\text{stat}) \pm 0.02(\text{syst})$ integrated over the kinematic range, i.e. $\langle Q^2 \rangle = 2.2 \text{ GeV}^2$, $\langle \text{Bjorken-}x \rangle = 0.15$, and $\langle -t \rangle = 0.4 \text{ GeV}^2$.

In the case of electroproduction from a target polarized longitudinally with respect to the lepton beam momentum, a small (at Hermes about 20%) transverse component (S_{\perp}) of the target polarization with respect to the direction of the virtual photon is present along with the dominating longitudinal component ($S_{||}$). According to Ref.⁶⁹, $A_{\text{UL}}^{\sin\phi}$ occurs in the polarized cross section σ_S of the reaction

$$\sigma_S \sim [S_{\perp} \sigma_{\mathcal{L}} + S_{||} \sigma_{\mathcal{L}\mathcal{T}}] A_{\text{UL}}^{\sin\phi} \sin\phi, \quad (23)$$

where contributions arise from the longitudinal (\mathcal{L}) amplitude and from the interference ($\mathcal{L}\mathcal{T}$) of longitudinal and transverse (\mathcal{T}) photon amplitudes, the latter being suppressed by $1/Q$ relative to $\sigma_{\mathcal{L}}$. However, both terms in Eq. 23 are expected to contribute at the same order in $1/Q$ since $\sigma_{\mathcal{L}}$ is weighted with the $1/Q$ suppressed transverse spin component S_{\perp} . For a complete interpretation of the measured asymmetry quantitative predictions for the term $\sigma_{\mathcal{L}\mathcal{T}}$ are required which rely on next-to-leading twist calculations⁷⁰. The upcoming Hermes data on a transversely polarized hydrogen target¹⁴ are important for further theoretical understanding and a decomposition of the contributions from the two target spin components.

7 Transversity and Prospects of Current Experiments

Regarding new experiments one of the most interesting questions is to determine the still unknown third type of twist-two quark distribution function δq , called transversity, first mentioned in Ref.⁷¹. In order to probe the transverse spin polarization of the nucleon, a helicity (identical to chirality at leading twist) flip of the struck quark must have occurred. In hard processes this is only possible with non-zero quark masses, thus suppressing this function in inclusive deep inelastic scattering. However, in semi-inclusive processes it is possible to combine two chiral odd parts, one describing the quark content of the target (δq) and another one describing the quark fragmentation into hadrons. Considerable effort has gone into understanding, modelling and proposed measures of δq , for a review see e.g. Ref.⁷².

There are important differences to be noted between the helicity and the transversity distributions which give further insight into the non-perturbative QCD regime of hadronic physics. For example, as mentioned before, quark and gluon helicities mix under Q^2 evolution, but there is no analog of gluon transversity in the nucleon. Furthermore, the difference between Δq and δq reflects the relativistic character of quark motion in the nucleon. Only in the case of non-relativistic movement of quarks in the nucleon are Δq and δq identical, i.e. invariant under a series of boosts and rotations which convert the longitudinally polarized nucleon into a transversely one. The first moments of the transversity distributions for quarks and anti-quarks are related to the flavor dependent contribution to the nucleon tensor charge $\delta\Sigma$, which behaves as a non-singlet matrix element⁷³. Hence the tensor charge is expected to be a more quark-model-like quantity in contrast to the axial charge, but more difficult to predict⁷⁴.

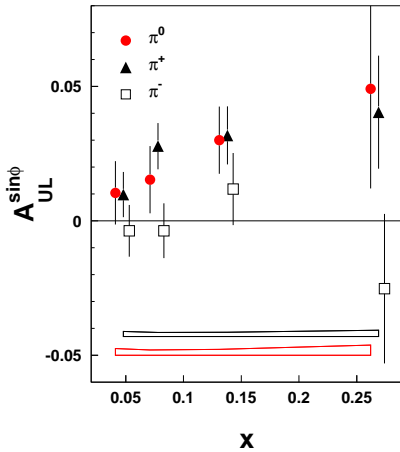


Figure 11. Analyzing power in the $\sin \phi$ moment for Hermes data on semi-inclusive charged⁷⁵ (systematic uncertainty: lower band) and neutral⁷⁶ (systematic uncertainty: upper band) pion production on a longitudinally polarized hydrogen target.

The recent observation of non-zero single-spin azimuthal asymmetries for neutral and positively charged pions by the Hermes collaboration generated much interest, since it can be interpreted as evidence for a non-zero chirality-flipping fragmentation function that couples to the quark transversity distributions. The results^{75,76} are presented in Fig.11, see also the left panel of Fig.10 and $z < 0.7$. The data were taken with a longitudinally polarized target which makes the interpretation of the Hermes results difficult due to possible additional twist-three contributions.

The study of transversity distributions and chiral-odd fragmentation functions, at least for the up-quark with good precision, is a primary goal of the Hermes Run II¹⁴ using a transversely polarized hydrogen target. Transversity is also an important part of ongoing and forthcoming experiments, see Ref. ⁷⁷ for an overview of the experimental state of the field. At BNL-RHIC interesting processes involving transversity in pp collisions are Drell-Yan lepton pair production with two protons transversely polarized or alternatively, chiral-odd two-pion interference

fragmentation in large p_T pion pair production using one proton transversely polarized.

The COMPASS⁷⁸ experiment at CERN has a transversity programme similiar to that of Hermes covering a different kinematic region. The primary goal of the COMPASS muon programme is the measurement of the gluon polarization $\Delta G/G$ with ~ 0.1 accuracy via open charm production and hadron pair production at large p_T for $0.04 < x_G < 0.3$ about.

Using both colliding proton beams longitudinally polarized, prompt photon production will be employed at RHIC to measure the helicity-dependent gluon density ΔG , at $0.02 < x_G < 0.3$ ⁷⁹. A compilation of simulated statistical accuracies for $\Delta G/G$ may be found e.g. in Ref.⁸⁰. It is important that various channels for extracting ΔG in eN- and pp-scattering are required to minimize the (so far strong) model-dependencies.

Alternatively to the Hermes programme to measure the flavor separated quark distributions, the production of weak W^\pm bosons in high energy polarized pp collisions at RHIC provides sensitivity to the quark and antiquark spin distributions⁸¹. The maximal parity violation in the interaction and the dependence of the production on the weak charge of the quarks may be used to select the specific flavor and charge of the quarks.

8 Concluding Remarks

Spin physics remains an exciting, rapidly developing field of research and contributes remarkably to the QCD picture of the structure of the nucleon. Recent precise spin structure function data from DESY and SLAC together with previous data improve the knowledge about the contribution of valence quarks to the nucleon spin within the framework of NLO pQCD and allow the fundamental Bjorken sum rule to be tested. Newest semi-inclusive double-spin asymmetry data from Hermes deliver additional sensitivity re-

quired for a complete flavor separation of polarized parton distributions, so far in LO pQCD. The contribution of gluons to the nucleon spin is not yet well known. It is suggested to be positive from LO/NLO pQCD fits based on inclusive DIS data and from a LO pQCD interpretation of Hermes high p_T hadron pair production data. A recent interesting development in QCD spin physics was triggered by the Hermes measurement of single-spin azimuthal asymmetries in semi-inclusive pion electroproduction off a longitudinally polarized target. This observation suggests a non-zero chiral-odd fragmentation function which allows one to access the so far unknown quark transversity distribution in semi-inclusive scattering from transversely polarized targets. For the first time, a window may be opened to access angular momenta of partons using the framework of generalized parton distribution functions based on new data on spin-dependent, hard exclusive processes, released by the Hermes and CLAS collaborations. Further experimental studies of the connection of semi-inclusive with exclusive reactions, and of high energy with low energy spin physics are being performed at JLAB and at DESY.

More precise data are expected to soon become available on the gluon spin, on the flavor separated quark and anti-quark helicities and on transversity properties from the high luminosity experiments at CERN, DESY, JLAB and RHIC-Spin, and also from an upcoming SLAC experiment ⁸². The perspectives also of future polarized lepton-nucleon fixed-target ^{80,83} and collider ⁸⁴ experiments are being discussed intensively. The goal remains to be the development of a complete, firm theoretically picture of the momentum and spin structure of hadrons.

Acknowledgment

I would like to thank D. Ryckbosch and E. Kinney for carefully reading this manuscript.

Many thanks to Juliet Lee-Franzini and her wonderful team for organizing such an inspiring conference.

References

1. E80 Collaboration, M. J. Alguard et al., *Phys. Rev. Lett.* **37**, 1261 (1976), *Phys. Rev. Lett.* **41**, 70 (1976).
2. E130 Collaboration, G. Baum et al., *Phys. Rev. Lett.* **51**, 1135 (1983); *Phys. Rev. Lett.* **45**, 2000 (1980).
3. European Muon Collaboration, J. Ashman et al., *Phys. Lett.* B **206**, 364 (1988); *Nucl. Phys.* B **328**, 1 (1989).
4. E142 Collaboration, P. L. Anthony et al., *Phys. Rev. D* **54**, 6620 (1996).
5. E143 collaboration, K. Abe et al., *Phys. Rev. D* **58**, 112003 (1998).
6. E154 Collaboration, K. Abe et al., *Phys. Rev. Lett.* **79**, 26 (1997).
7. E155 Collaboration, P. L. Anthony et al., *Phys. Lett.* B **463**, 339 (1999).
8. E155 Collaboration, P.L. Anthony et al., *Phys. Lett.* B **493**, 19 (2000).
9. Spin Muon Collaboration, B. Adeva et al., *Phys. Rev. D* **58**, 112001 (1998).
10. HERMES Collaboration, K. Ackerstaff et al., *Phys. Lett.* B **404**, 383 (1997).
11. HERMES Collaboration, A. Airapetian et al., *Phys. Lett.* B **442**, 484 (1998).
12. S. Rock for the E155X Collaboration, see in Ref. ⁷⁷.
13. P. Lenisa for the Hermes Collaboration, see in Ref. ⁸⁵.
14. M. G. Vincter for the Hermes Collaboration, see in Ref. ⁷⁷.
15. COMPASS, *A Proposal for a CCommon Muon and Proton Apparatus for Structure and Spectroscopy*, CERN/SPSLC 96-14, SPSLC/P27, 1 March 1996.
16. E. M. Kabuss for the COMPASS Collaboration, see in Ref. ⁸⁶.
17. Polarized Proton Collider at RHIC, <http://www.agsrhichome.bnl.gov/RHIC/Spin>.

18. PHENIX Collaboration, Y. Akiba et al., *Nucl. Phys. A* **638**, 565 (1998).
19. STAR Collaboration, K. H. Ackermann et al., *Nucl. Phys. A* **661**, 681 (1999).
20. J. Soffer, and O. V. Teryaev, *Phys. Lett. B* **490**, 106 (2000).
21. J. L. Friar et al., *Phys. Rev. C* **42**, 2310 (1990).
22. C. Ciofi degli Atti et al., *Phys. Rev. C* **48**, 968 (1993).
23. R. Blankleider and R. M. Woloshyn, *Phys. Rev. C* **29**, 538 (1984).
R. W. Schulze and P. U. Sauer, *Phys. Rev. C* **48**, 38 (1993).
24. M. Lacombe et al., *Phys. Lett. B* **101**, 139 (1981).
25. P. Hoodbhoy, R. L. Jaffe and A. Manohar, *Nucl. Phys. B* **312**, 571 (1989).
K. Bora, and R. L. Jaffe, arXiv: hep-ph/9711323 (1997).
26. U. Stößlein for the Hermes Collaboration, see in Ref. ⁸⁵.
27. Spin Muon Collaboration, B. Adeva et al., *Phys. Rev. D* **60**, 072004 (1999).
28. Spin Muon Collaboration, D. Adams et al., *Phys. Lett. B* **336**, 125 (1994).
29. E143 Collaboration, K. Abe et al., *Phys. Rev. Lett.* **76**, 587 (1996).
30. E154 Collaboration, K. Abe et al., *Phys. Lett. B* **404**, 377 (1997).
31. E155 Collaboration, P.L. Anthony et al., *Phys. Lett. B* **458**, 530 (1999).
32. W. Wandzura, and F. Wilczek, *Phys. Lett. B* **172**, 195 (1977).
33. B. W. Filippone and X. Ji, arXiv: hep-ph/0101224.
34. Y. R. Roblin for the GDH Collaboration, see in Ref. ⁸⁶.
35. G. Dodge for the CLAS Collaboration, to appear in Ref. ⁸⁷.
36. H1 Collaboration, C. Adloff et al., *Eur. Phys. J. C* **21**, 33 (2001).
37. H. Abramowicz and A. Levy, arXiv: hep-ph/9712415 (1997).
38. L. W. Withlow et al., *Phys. Lett. B* **250**, 193 (1990).
39. E. Leader, A.V. Sidorov, D. Stamenov, *Phys. Lett. B* **445**, 232 (1998).
40. Spin Muon Collaboration, B. Adeva et al., *Phys. Rev. D* **58**, 112002 (1998).
41. J. Blümlein and H. Böttcher, to appear in Ref. ⁸⁷.
42. M. Glück et al., arXiv: hep-ph/0011215 (2000).
43. Asymmetry Analysis Collaboration, Y. Goto et al., *Phys. Rev. D* **62**, 034017 (2000), arXiv: hep-ph/0001046 (2000).
44. E154 Collaboration, K. Abe et al., *Phys. Lett. B* **405**, 180 (1997).
45. J. Ellis and R. Jaffe, *Phys. Rev. D* **9**, 1444 (1974); 1016691974 (E.).
46. E. Leader, A.V. Sidorov, D. Stamenov, arXiv: hep-ph/0106214 (2001).
47. Hermes Collaboration, A. Airapetian et al., *Phys. Rev. Lett.* **84**, 2584 (2000).
48. T. Gehrmann, W. J. Stirling, *Phys. Rev. D* **53**, 6100 (1996).
49. M. Glück et al., *Phys. Rev. D* **53**, 4775 (1996).
50. T. Sjöstrand, *Comp. Phys. Comm.* **82**, 74 (1994). PYTHIA version 5.724.
51. E. C. Aschenauer for the Hermes Collaboration, to appear in Ref. ⁸⁷.
52. Spin Muon Collaboration, B. Adeva et al., *Phys. Lett. B* **420**, 180 (1998).
53. Hermes Collaboration, K. Ackerstaff et al., *Phys. Lett. B* **464**, 123 (1999).
54. T. Lindemann for the Hermes Collaboration, see in Ref. ⁸⁵.
55. G. Ingelman, A. Edin, J. Rathsman, DESY Report 96-057 (1996).
56. K. Goeke et al., arXiv: hep-ph/0001272 (2000).
57. M. Stratmann and W. Vogelsang, arXiv: hep-ph/0107064 (2001).
58. K. Goeke, M. V. Polyakov, M. Vanderhagen, *Prog. Part. Nucl. Phys.* **47**, 401 (2001).
59. X. Ji, *Phys. Rev. Lett.* **78**, 610 (1997), arXiv: hep-ph/9603249 (1996).
60. R. L. Jaffe and A. Manohar, *Nucl. Phys.*

B **337**, 509 (1990).

61. R. L. Jaffe, arXiv: hep-ph/0102281 (2001).

62. A. V. Belitsky, D. Müller, arXiv: hep-ph/0111037 (2001).

63. E. R. Berger et al., arXiv: hep-ph/0106192 (2001).

64. Hermes Collaboration, A. Airapetian et al., *Phys. Rev. Lett.* **87**, 182001 (2001).

65. CLAS Collaboration, S. Stepanyan et al., *Phys. Rev. Lett.* **87**, 182002 (2001).

66. L. L. Frankfurt et al., *Phys. Rev. Lett.* **84**, 2589 (2000).

67. H. Avakian for the Hermes Collaboration, see in Ref. ⁸⁶.

68. Hermes Collaboration, A. Airapetian et al., arXiv: hep-ex/011202, submitted to *Phys. Lett. B*.

69. M. V. Polyakov, M. Vanderhaeghen, see in Ref. ⁸⁶.

70. A. V. Belitsky, D. Müller, *Phys. Lett. B* **513**, 349 (2001).

71. J. P. Ralston, D. E. Soper, *Nucl. Phys. B* **152**, 109 (1979).

72. V. Barone, A. Drago, P. G. Ratcliffe, arXiv: hep-ph/0104283 (2001).

73. R. L. Jaffe, X. Ji, *Phys. Rev. Lett.* **67**, 552 (1991); *Nucl. Phys. B* **375**, 527 (1992).

74. L. Gamberg, G. R. Goldstein, arXiv: hep-ph/0107176 (2001).

75. Hermes Collaboration, A. Airapetian et al., *Phys. Rev. Lett.* **84**, 4047 (2000).

76. Hermes Collaboration, A. Airapetian et al., *Phys. Rev. D* **64**, 097101 (2001).

77. Proceedings of the Topical Workshop on Transverse Spin Physics July 2001, Zeuthen Germany, <http://www-zeuthen.desy.de/spin01>.

78. F.-H. Heinsius for the COMPASS Collaboration, to appear in Ref. ⁸⁷.

79. L. Bland, see in Ref. ⁷⁷.

80. W.-D. Nowak, arXiv: hep-ph/0111218 (2001).

81. S. E. Vigdor for the STAR Collaboration, see in Ref. ⁸⁵.

82. E161 Collaboration, *Measurement of the Polarized Gluon Distribution Using Open Charm Production*, <http://www.slac.stanford.edu/exp/e161>

83. D. Ryckbosch, to appear in Ref. ⁸⁷.

84. Proceedings of the 2th Workshop on Physics with a Polarized-Electron Light-Ion Collider, September 2000, MIT Cambridge, MA USA, Melville New York 2001, AIP conference proceedings Vol. 588.

85. Proceedings of the 14th International Spin Physics Symposium (SPIN2000), October 2000, Osaka Japan, Melville New York 2001, AIP conference proceedings Vol. 570.

86. Proceedings of the 8th International Workshop on Deep-Inelastic Scattering, April 2000, Liverpool UK, World Scientific 2000.

87. Proceedings of the 9th International Workshop on Deep Inelastic Scattering, April 2001, Bologna Italy, 2001.